Received: 25 May 2020 | Revised: 23 September 2020 | Accepted: 3 October 2020

DOI: 10.1002/joc.6865

RESEARCH ARTICLE

International Journal of Climatology RMetS

Changes in daily extreme temperature and precipitation events in mainland China from 1960 to 2016 under global warming

Xuyang Wang[1,3] | Yuqiang Li[1,2,3] | Mingming Wang[1,2] | Yulin Li[1,2,3] | Xiangwen Gong[1,2] | Yinping Chen[4] | Yun Chen[1,2] | Wenjie Cao[4]

[1]Northwest Institute of Eco-Environment and Resources, Chinese Academy of Sciences, Lanzhou, China

[2]University of Chinese Academy of Sciences, Beijing, China

[3]Naiman Desertification Research Station, Northwest Institute of Eco-Environment and Resources, Chinese Academy of Sciences, Tongliao, China

[4]School of Environmental and Municipal Engineering, Lanzhou Jiaotong University, Lanzhou, China

Correspondence
Yuqiang Li, Northwest Institute of Eco-Environment and Resources Chinese Academy of Sciences, 320 Donggang West Road, Lanzhou, 730000, China.
Email: liyq@lzb.ac.cn

Funding information
National Key R and D Program of China, Grant/Award Numbers: 2017YFA0604803, 2016YFC0500901; National Natural Science Foundation of China, Grant/Award Numbers: 31971466, 41807525; Strategic Priority Research Program of the Chinese Academy of Sciences, Grant/Award Number: XDA23060404

Abstract

Extreme climatic events have become a global concern. Understanding changes in these events is essential to support efforts to reduce their impacts. We investigated the spatial and temporal variation of 15 temperature and 11 precipitation extremal indices based on daily observations from 1960 to 2016 at 794 meteorological stations in mainland China. The regionally averaged temperature index trends were consistent with global warming. An abrupt change in the trends for warmth-related indices mainly occurred from 1990 to 2000, and the year with an abrupt change for cold-related indices appeared earlier (mainly around 1990). The numbers of warm days, warm nights, summer days, and tropical nights increased significantly. In contrast, the numbers of cool days, cool nights, ice days, and frost days decreased significantly. The coldest night temperature had a strong and significant warming trend (0.4°C·decade^{-1}), whereas the number of frost days showed the fastest decrease (2.6 days·decade^{-1}). The warmth and extremal indices decreased significantly with increasing latitude, whereas warming trends increased significantly with increasing longitude, and the warmth indices and extremal daily indices decreased with increasing elevation. The number of consecutive wet days decreased fastest, at 0.09 days·decade^{-1}, and the daily intensity index increased fastest, at 0.09 mm·day^{-1} per decade. The extreme precipitation events decreased significantly with increasing latitude, but increased with increasing longitude. Large-scale atmospheric circulation indices (the Arctic Oscillation and the Western Pacific Subtropical High Intensity and Area indices) and the Western Ridge Point strongly influenced the warm and cold extremes and contributed significantly to climate change in mainland China. The Western Ridge Point and Subtropical High Area were the dominant drivers of extreme temperature and precipitation events, respectively, in mainland China.

KEYWORDS

atmospheric circulation, extreme climatic events, precipitation, subtropical high, temperature

1 | INTRODUCTION

Global climate change is no longer disputed, and the Fifth Assessment Report (AR5) of the Intergovernmental Panel on Climate Change (IPCC) reported that the global average surface temperature increased by 0.85°C from 1880 to 2012 (IPCC, 2013). Global temperatures in 2016 were 1.2°C above preindustrial levels according to an assessment by the World Meteorological Organization (WMO, 2016). Although these averages are important, climate change also affects the magnitude and frequency of extreme weather and extreme climatic events such as heat waves, storms, hailstorms, tornadoes, and hurricanes. These changes have greatly affected agriculture, energy consumption, ecosystems, and human health around the world (IPCC, 2013).

In recent years, extreme summer heat waves have occurred frequently, including in Europe in 2003 (Luterbacher, 2004), Southern Europe in 2007 (Founda and Giannakopoulos, 2009), Australia's Victoria State in 2009 (Karoly, 2009), Western Russia in 2010 (Barriopedro *et al*., 2011), and North America in 2011 (Coumou and Rahmstorf, 2012). Warming increases evaporation from the soil surface, thereby drying the surface soil and increasing the intensity and duration of drought (Trenberth, 2011; Mazdiyasni and AghaKouchak, 2015). Extensive droughts occurred in the central and northern United States in 2012 (Hoerling *et al*., 2014) and 2017 (Gerken *et al*., 2018), southern China in 2013 (Yuan *et al*., 2015), and southern Africa in 2015 (Yuan *et al*., 2018). Widespread drought threatens water and food security, environmental sustainability, and even human life (Hoerling *et al*., 2014), and may cause heat waves or wildfires that trigger compound extreme events (Mueller and Seneviratne, 2012; Zscheischler *et al*., 2018), such as the catastrophic 2019 wildfires in southeastern Australia.

During this same period, warming has also increased the atmosphere's water vapour content because the air's water holding capacity increases by 7% for each 1°C increase, thereby producing more intense precipitation (Trenberth, 2011). Record rainfall has been recorded in many regions, including Central Europe in 2002 (Becker and Grünewald, 2003), the South Atlantic in 2004 (Pezza and Simmonds, 2005), Pakistan in 2010 (Webster *et al*., 2011), and the northeastern United States, Western Europe, Japan, and Korea in 2011 (WMO, 2011). Extreme precipitation events cause uneven distribution of precipitation, leading to extreme hydrological events such as floods or droughts, which significantly affect a region's economy and residents, especially in developing countries where income and survival depend mainly on agriculture (Zhang *et al*., 2005).

Furthermore, compared with gradual changes in the mean climate, extreme weather or climate events appear to be more sensitive to global climate change, and have greater potential to cause disastrous impacts on a region's economy and residents, as well as on its ecological environment (Meehl *et al*., 2000; IPCC, 2014). To support efforts to mitigate the consequences of these changes, it is necessary to understand their spatial and temporal trends so that governments can predict future changes in the extremes. Thus, studies to detect changes in climate extremes have received widespread attention around the world. At a global scale, the studies of climate extremes by Groisman *et al*. (1999) and Frich *et al*. (2002) lacked sufficient data on Central and South America, Africa, and southern Asia, leading to large uncertainty in their findings. Kiktev *et al*. (2003) analysed six climate extremal indices based on updates of Frich *et al*.'s (2002) dataset, but the spatial coverage of meteorological data sites was still poor. Subsequent studies such as Alexander *et al*. (2006) found that more than 70% of the global land area exhibited a significant increase in the number of warm nights and a significant decrease in the number of cold nights from 1951 to 2003.

Because changes in climate extremes differ among regions, studies of these changes were conducted on a large scale in different regions, including Europe (Klein Tank and Können, 2003), Central and South America (Aguilar *et al*., 2005), the Asia-Pacific region (Griffiths *et al*., 2005), and Africa (New *et al*., 2006; Gbode *et al*., 2019). Almost all results showed that widespread changes in temperature extremes were closely linked with global warming, and that precipitation extremes exhibited higher spatial variability than temperature extremes.

In China, warmth indices, including the numbers of warm days, warm nights, and summer days, have generally increased, whereas cold indices, including the numbers of frost days, cold days, and cold nights, have generally decreased in frequency and intensity, with varying magnitudes of change across China's diverse regions (Li *et al*., 2011; Zhen and Li, 2014; Guan *et al*., 2015; Zhong *et al*., 2017). The numbers of extreme precipitation events have increased in southern, southwestern, and northern China, but have decreased in central, northwestern, and northeastern China (Ning *et al*., 2012; Lu *et al*., 2014; Li *et al*., 2015; Sun *et al*., 2016). However, these studies were limited by their reliance on relatively few meteorological stations and an insufficient study period. In the IPCC Assessment Report (Houghton *et al*., 2001), China was described as a data-sparse area that limited the ability to describe global trends in precipitation from 1976 to 1999. Thus, it has become increasingly necessary to provide a more thorough account of changes in extreme temperature and precipitation in China and cover a longer period, especially to provide an update on the changes that have occurred since 1999.

Based on this context, the main objectives of the present study were to (a) detect trends in indices for extremes in daily temperature and precipitation throughout China from 1960 to 2016, (b) explore the spatial variation in extreme temperature and precipitation events (with respect to latitude, longitude, and elevation), and (c) identify relationships between these dynamic changes in the extreme climate indices and global atmospheric circulation patterns.

2 | DEFINITIONS AND METHODS

2.1 | Data

We obtained quality-controlled data, including daily maximum temperature (TX), minimum temperature (TN), and daily precipitation (PRCP) from 839 meteorological stations distributed throughout China (Figure 1), with data obtained from the National Climate Center of the China Meteorological Administration (http://data.cma.cn). The quality and completeness of the dataset have significantly improved as a result of strict quality control, and we selected a total of 794 sites that had <10% missing data for the period from 1960 to 2016. However, for the present study, it is worth noting that as shown in Figure 1, the results of extreme climate change are not representative in parts of the Southwest and Northwest due to the sparsely distributed meteorological stations.

Because the climate extreme indices differ among stations, instruments, and data collection procedures (Haylock *et al*., 2006), we performed further quality control before calculating the extremal indices. For quality control, we (a) replaced all missing values (originally coded as −99.9) with an internal format recognized by the R statistical software (i.e., NA, for not available), and (b) replaced all unreasonable values with NA. Examples of unreasonable data include a daily minimum temperature that was higher than the daily maximum temperature and a daily rainfall that was <0 mm. In addition, we identified outliers in daily maximum and minimum temperatures, which we defined as daily values that lay outside a range defined as n times the standard deviation (STD) of the value for that day; that is, we included only values in the range (mean − 3 STD, mean + 3 STD).

To detect artificial multiple change points (shifts) in a data series, we conducted homogeneity assessments for the recorded daily temperature and precipitation data from 1960 to 2016. We used version 4 of the RHtests software developed by Wang and Feng at the Climate Research Branch of the Meteorological Service of Canada (http://etccdi.pacificclimate.org/software.shtml) to detect and adjust first-order autoregressive errors caused by shifts. The RHtests package was applied using the penalized maximal t test (Wang *et al*., 2007) and the penalized maximal F test (Wang, 2008b), which are embedded in a recursive testing algorithm that accounts empirically for a lag −1 autocorrelation (if any) in the time series (Wang, 2008a).

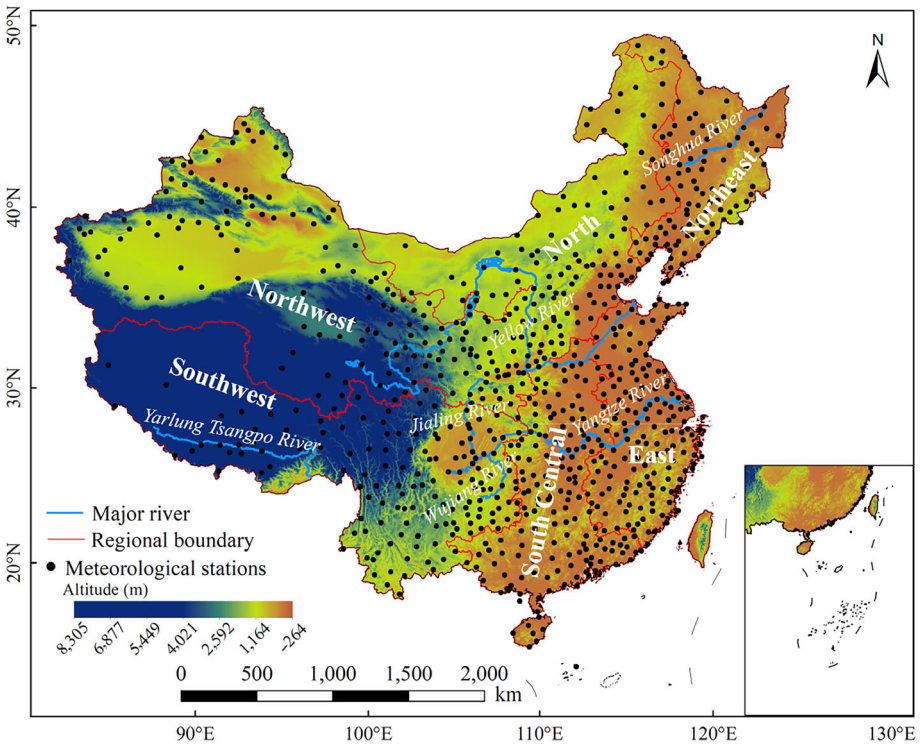

FIGURE 1 Study area and the distribution of the 794 Chinese meteorological stations used in the present study. The study area was divided into six regions: northwest, north, northeast, southwest, south central, and east

2.2 | Definitions

To facilitate monitoring and analysis of changes in the intensity, frequency, and duration of the extreme temperature and precipitation events in different parts of the world, the Expert Team on Climate Change Detection and Indices (http://cccma.seos.uvic.ca/ETCCDI/), led by the World Meteorological Organization, defined a core suite of 26 extreme climate indices (15 temperature and 11 precipitation indices; Table S1), as well as related software for their calculation (Powell and Keim, 2015). These climate indices were also recommended by the Climate Change and Predictability Program's Climate Change Detection group, the Global Climate Research Program, and the Climate Commission of the World Meteorological Organization (Wang *et al*., 2018). During the last several years, these indices have been widely applied throughout the world (Klein Tank and Können, 2003; Aguilar *et al*., 2005; Dos Santos *et al*., 2011; Croitoru *et al*., 2013; Insaf *et al*., 2013; Guan *et al*., 2015; Filahi *et al*., 2016; Sun *et al*., 2016; Supari *et al*., 2016; Gbode *et al*., 2019). The specific definitions of the 26 climate indices and their development are described by Alexander *et al*. (2006), Klein Tank *et al*. (2009), and Donat *et al*. (2013), and on the relevant Web site (http://www.climdex.org). The temperature indices comprise 7 cold-related indices and 8 warmth-related indices, and these indices can be further grouped according to their method of calculation as 4 percentile, 4 threshold, 4 extremal indices, and 3 duration indices. The precipitation indices comprise 1 dry index and 10 wet indices, which can be grouped into 2 percentile, 3 threshold, 2 duration, 2 extremal, and 2 other indices (Powell and Keim, 2015).

2.3 | Atmospheric circulation patterns

To analyse the influence of the main atmospheric circulation types on temperature and precipitation extremes in mainland China, we calculated Pearson's *r* for the relationships between the climate extreme indices and the following atmospheric circulation indices: the Arctic Oscillation (AO), North Atlantic Oscillation (NAO), Southern Oscillation Index (SOI), and Pacific Decadal Oscillation (PDO). We obtained this data from the National Oceanic and Atmospheric Administration (http://www.esrl.noaa.gov/psd/data/climateindices/list/). In addition, we selected four components of the West Pacific Subtropical High Index (WPSHI): the Subtropical High Intensity (SHI) index, Subtropical High Area (SHA) index, Subtropical High Western Ridge Point (SHW) index, and Subtropical High Ridge Line (SHR) index. We obtained this data from the Climate Diagnostics and Prediction Division, National Climate Center, China Meteorological Administration (http://cmdp.ncc-cma.net/Monitoring/). SHI and SHA represent the intensity and area of the West Pacific Subtropical High, respectively, whereas SHW and SHR represent the position and direction of the Western Ridge Point and Ridge Line. When SHW increases, this means that the Western Ridge Point is located more towards the east, and when SHW increases, this means that the Ridge Line of the WPSHI is located more towards the north.

2.4 | Statistical analysis

We used least-squares linear regression to calculate the slopes of the trends for the climate indices from 1960 to 2016. We used the Mann–Kendall test (Kendall, 1990) to detect significant trends and abrupt changes for climate extreme indices; this nonparametric trend test is suitable for data that may not be normally distributed, and is less sensitive to the effects of outliers (Tabari *et al*., 2011). This method has been widely used to analyse time series to detect trends in meteorological and hydrological data (Viola *et al*., 2014; Sun *et al*., 2016; Supari *et al*., 2016; Zhong *et al*., 2017). We used the Z statistic to judge the direction of the trends and their significance; $Z > 0$ represents an increasing trend, whereas $Z < 0$ represents a decreasing trend. When the absolute value of Z is greater than or equal to 1.96, 2.58, and 3.30, the trend is significant at $p < .05$, .01, and .001, respectively (Hamed and Rao, 1998). We used ordinary kriging interpolation in version 10.3 of the ArcMap software (http://www.esri.com) to define the spatial pattern of trends in the climate indices. We used Pearson's correlation coefficient (r) to detect significant relationships among the extremal variables and between extreme climate events and atmospheric circulation patterns. Furthermore, we used a constrained ordination method (redundancy analysis, RDA) to assess the influence of the atmospheric circulation patterns on climate extremes, and produced the ordinations using version 5.0 of the Canoco software (http://www.canoco5.com/).

3 | RESULTS

3.1 | Nationwide trends for the temperature and precipitation extremal indices

During the study period from 1960 to 2016, the majority of stations showed decreases for the cold temperature indices (Figure 2): the numbers of cool days (TX10p), cool nights (TN10p), ice days (ID), and frost days (FD) decreased at

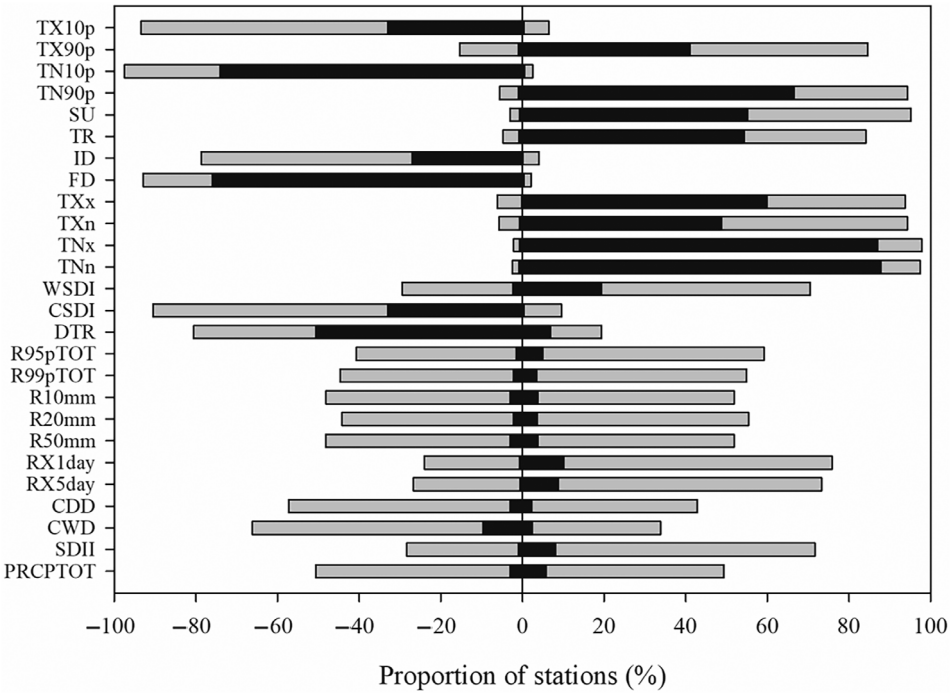

FIGURE 2 Proportions of the meteorological stations in China that showed increases or decreases in the extremal climate indices from 1960 to 2016. Black portions of the bar represent stations at which the trend was statistically significant at $p < .05$. The descriptions of the indices and proportions of stations with positive or negative trends are shown in Table S1, respectively

TABLE 1 Results of the abrupt change in extreme climate events during 1960 to 2016 in mainland China

	Before abrupt change			After abrupt change	
Indices	***K***	**Mean**	**Abrupt year**	***K***	**Mean**
TX10p	−0.18	12.55	1992	−0.03	10.73
TX90p	0.08	11.46	2000	0.60	14.10
TN90p	0.28	11.07	1992	0.65	14.60
TN10p	−0.51	14.32	1986	−0.43	10.56
SU	0.73	115.99	2001	0.31	125.24
TR	0.82	56.95	1999	2.15	63.88
FD	−1.30	101.11	1993	−2.36	92.63
ID	−0.16	33.70	1988	0.13	29.91
DTR	−0.30	10.95	1975	−0.07	10.53
WSDI	0.17	10.17	2008	3.04	12.18
TXx	0.05	24.47	2000	0.17	25.21
TXn	−0.02	9.58	1993	0.10	10.22
TNx	0.10	12.78	1995	0.35	13.69
TNn	0.23	0.22	1990	0.27	1.38

Note: Indices are defined in Table S1. The *K* value represents the change trend before or after the year with the abrupt change (calculated using linear least-squares regression) and represents a change per decade.

93, 98, 79, and 93% of the stations, respectively. Conversely, most stations showed increased warm temperature indices: the numbers of warm days (TX90p), warm nights (TN90p), summer days (SU), and tropical nights (TR) increased at 85, 94, 95, and 84% of the stations, respectively. In addition, more than 90% of the stations showed increases in the extremal indices: warmest day (TXx), warmest night (TNx), coldest day (TXn), and coldest night (TNn). Roughly 81% of stations showed decreases in the diurnal temperature range (DTR), with 51% of the decreases being significant. For the duration indices, 90% of the stations showed decreases in the cold

spell duration (CSDI) and 71% of stations showed increases in the warm spell duration (WSDI), indicating that the duration of periods of extreme heat increased, and cold outbreaks became shorter.

In general, the precipitation indices showed fewer significant overall trends than existed for the temperature indices. For instance, 73% of stations showed increases in the maximum monthly 5-day precipitation (Rx5day), but with significant trends at only 9% of the stations. In addition, 59% of the stations showed increases in the amount of precipitation on very wet days (R95pTOT, >95th percentile), but only 5% had a significant trend, and 55% of stations showed increases in the number of very heavy precipitation days (R99pTOT, > 99th percentile), but only 4% had a significant trend. The monthly maximum 1-day precipitation (Rx1day) was most commonly significant; 76% of stations showed increases in this index, but only 10% of the stations showed a significant trend. Overall, the precipitation indices showed more significant increases than decreases, indicating that precipitation events became increasingly large or prolonged from 1960 to 2016.

Although the frequency and intensity of extreme events increased, the duration of extreme precipitation events appears to be decreasing. The two wet and dry duration indices, consecutive wet days (CWD) and consecutive dry days (CDD), showed more significant decreases than increases. Specifically, 66% of stations showed decreases in CWD, with 10% of the stations showing significant decreases, compared to 34% of stations that exhibited increases, but with only 2% of the stations showing a significant increase. Furthermore, roughly equal proportions of the stations showed increasing and decreasing trends in annual total precipitation on wet days (when daily rainfall >1 mm).

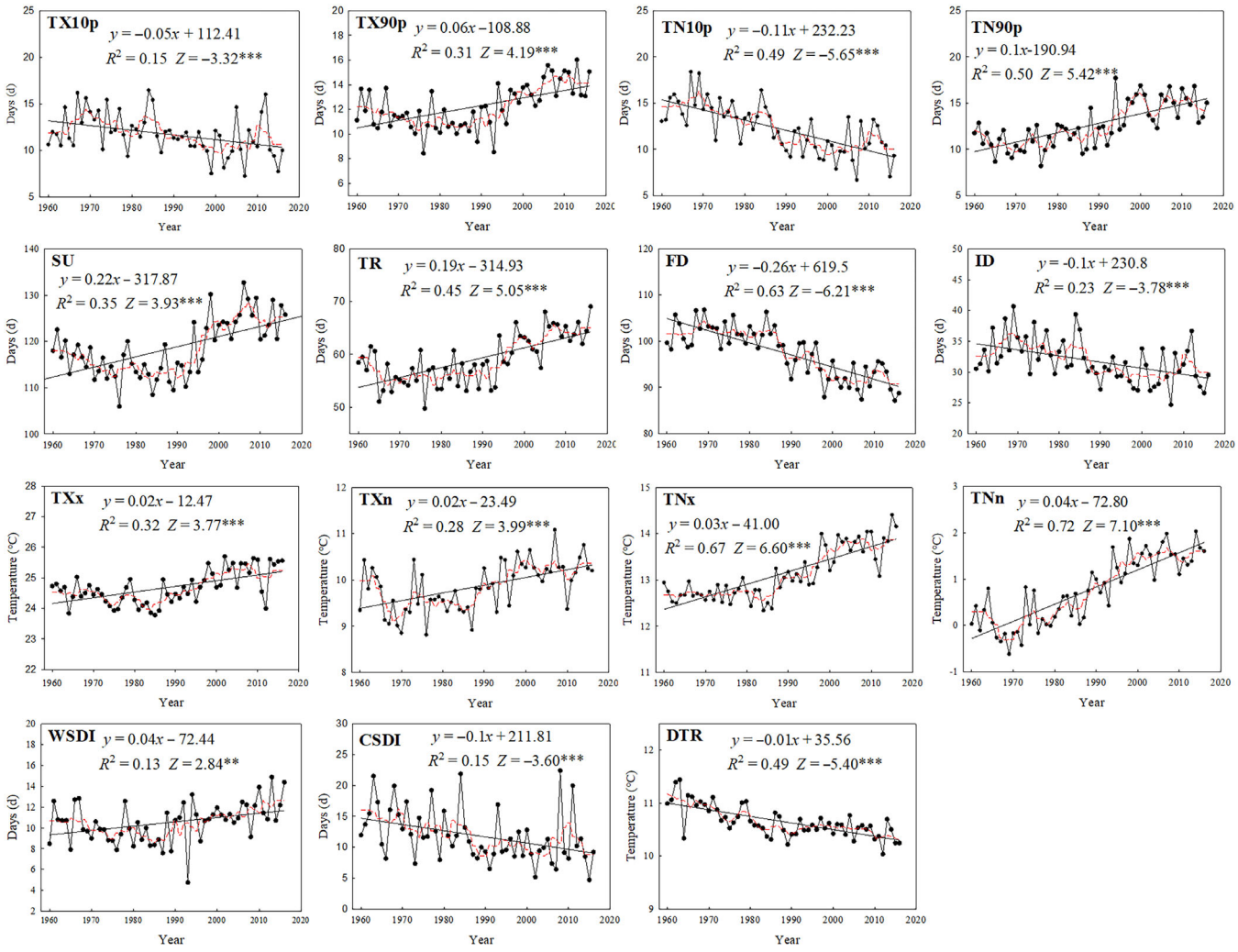

FIGURE 3 Regionally averaged series for indices of the extreme temperature events in China from 1960 to 2016. The indices are defined in Table S1. Straight lines represent statistically significant linear regressions; the dashed red line is the smoothed 5-year running average. Z scores represent the Mann–Kendall test results. Significance: ***$p < .001$; **$p < .01$

3.2 | Abrupt changes in trends for extreme climate events

We used the Mann–Kendall method to detect abrupt climate changes. The abrupt climate changes for warmth-related indices mainly occurred from 1990 to 2000 (Table 1). The abrupt changes in the numbers of warm days (TX90p), warm nights (TN90p), summer days (SU), tropical nights (TR), warmest day (TXx) and warmest night (TNx) occurred in 2000, 1992, 2001, 1999, 2000, and 1995, respectively. After the abrupt climate change, the increasing trend for these warmth-related indices accelerated, with the largest increase for TR (by 1.33 days·decade^{-1}). Moreover, the warm spell duration (WSDI) had an abrupt change in 2008, and its rate of increase also accelerated (by 2.87 days·decade^{-1}) after 2008. However, compared with the warmth-related indices, the abrupt changes for cold-related indices appeared earlier (mainly around 1990). The numbers of cool days (TX10p), cool nights (TN10p), ice days (ID), and frost days (FD), and the temperatures of the coldest day (TXn) and coldest night (TNn) changed abruptly in 1992, 1986, 1988, 1993, 1993, and 1990, respectively. After the abrupt change, the rate of decrease of TX10p and TN10p slowed (by 0.15 and 0.08°C·decade^{-1}, respectively), whereas the rate of decrease of FD accelerated (by 1.06 days·decade^{-1}) and the trends for ID and TXn changed to increases. In addition, the extreme

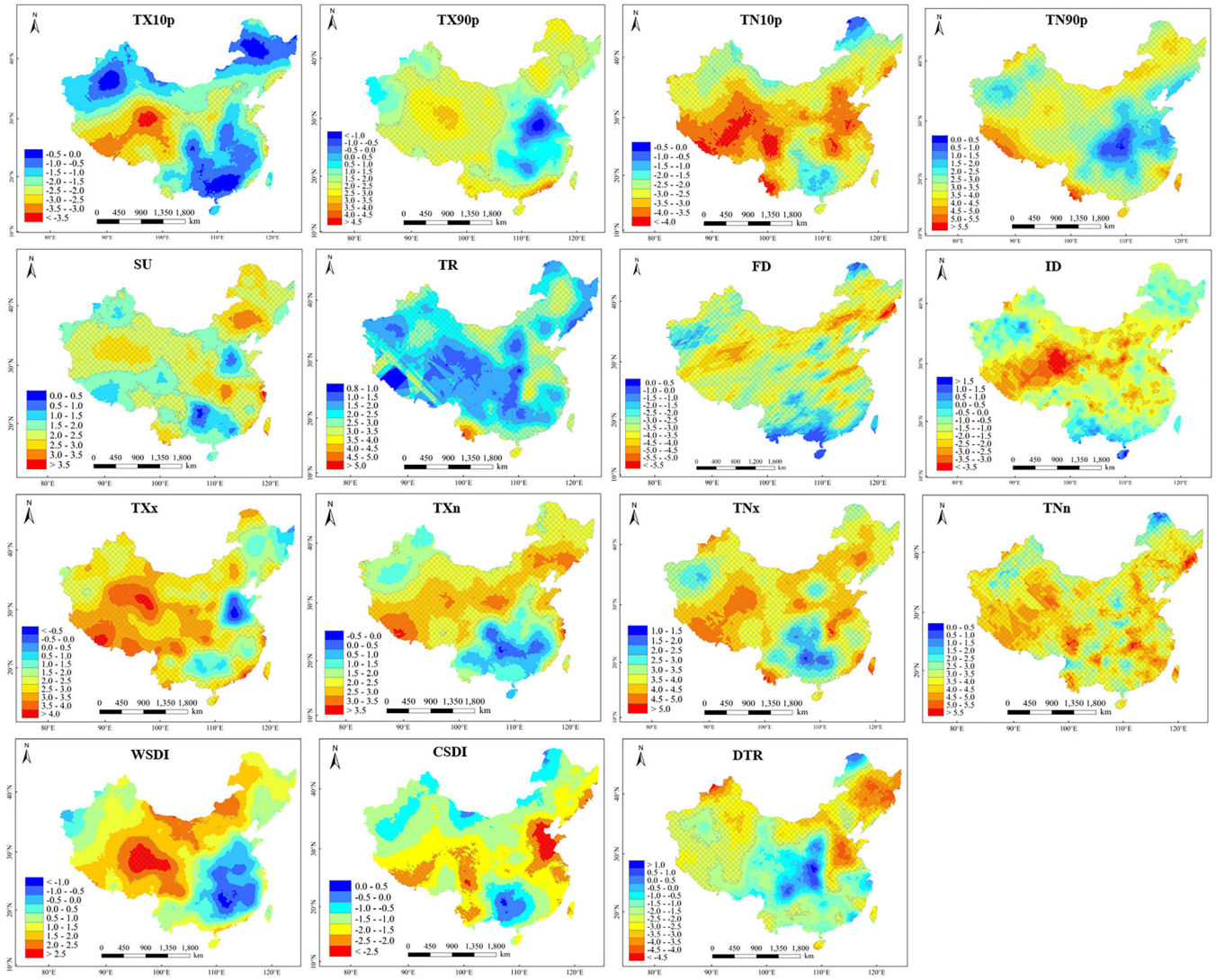

FIGURE 4 Spatial pattern of the Mann–Kendall Z values for temperature indices from the 794 meteorological stations in China from 1960 to 2016. The indices are defined in Table S1. $Z < 0$ represents a decreasing trend, $Z > 0$ represents an increasing trend, and $|Z| > 1.96$ represents a statistically significant trend ($p < .05$). Hatching shows areas where the change trends are significant

precipitation events showed no significant abrupt climate change.

3.3 | Trends for extreme temperature events

3.3.1 | Temporal trends of extreme temperature events

In China, the regionally averaged occurrence of warmth indices, including the numbers of warm days (TX90p), warm nights (TN90p), summer days (SU), and tropical nights (TR), increased significantly ($p < .001$), at rates of 0.6, 1.0, 2.2, and 1.9 days per decade, respectively (Figure 3). TN90p showed the strongest increase, with a Mann–Kendall test value of $Z = 5.42$. In contrast, the cold indices, including the numbers of cool days (TX10p), cool nights (TN10p), ice days (ID), and frost days (FD) decreased significantly ($p < .001$), at rates of 0.5, 1.1, 1.0, and 2.6 days per decade. The trend was strongest for FD ($Z = -6.21$). The extremal indices for the warmest day (TXx), warmest night (TNx), coldest day (TXn), and coldest night (TNn) showed significant warming trends, at rates of 0.2, 0.3, 0.2, and 0.4°C per decade ($p < .001$). TNn showed the strongest increasing trend, with a Mann–Kendall test value of $Z = 7.10$.

3.3.2 | Spatial trends in extreme temperature events

To further examine the trends in the temperature indices, we mapped the spatial patterns of the annual trends based on Mann–Kendall *Z*-values at the 794 meteorological stations (Figure 4). The numbers of warm days (TX90p) and warm nights (TN90p) generally decreased from west to east, with the weakest change trends in the South Central and East regions. From west to east, the number of cool nights (TN10p) increased initially, then decreased slightly and finally increased again. The area where the number of cool days (TX10p) decreased most significantly was mainly in the Southwest region, with weak trends in the Northwest, Northeast, and East regions. The trend for the number of summer days (SU) was strongest in the coastal areas of East China, and the number of tropical nights (TR) showed a similar pattern, but with much weaker trends, in most areas in the Southwest and Northwest. The number of frost days (FD) showed a significant decrease in most areas of China, whereas the number of ice days (ID) decreased most significantly in the Northwest region.

3.3.3 | Correlations among the temperature indices

Figure 5 presents the correlations among the temperature indices, including the mean annual temperature (Tem). Most of the extreme temperature indices were moderately to strongly correlated with the annual mean temperature, with correlation coefficients greater than .5 ($p < .05$), except for the diurnal temperature range (DTR). The warmth indices were significantly positively correlated with annual mean temperature, and the correlation coefficients ranged from .71 to .83. In contrast, we observed significant negative correlations between the cool indices and the annual mean temperature; the number of frost days had the strongest correlation (−.96) with the mean temperature. Furthermore, we found significant positive correlations among the warmth indices and among the cold indices.

3.4 | Trends for the extreme precipitation events

3.4.1 | Temporal trends for extreme precipitation events

The regionally averaged occurrence of daily intensity index (SDII) from 1960 to 2016 increased significantly, at a rate of 0.05 mm·day^{-1} per decade ($p < .001$) (Figure 6).

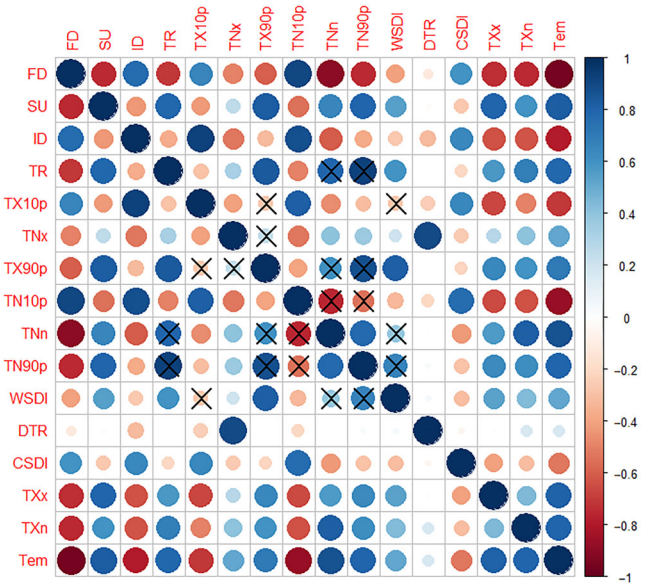

FIGURE 5 Correlations (Pearson's *r*) among the annual mean temperature and the extreme temperature indices from 1960 to 2016. Indices are defined in Table S1. The circle size is proportional to the *r* value, and the X symbol in a cell means a nonsignificant correlation

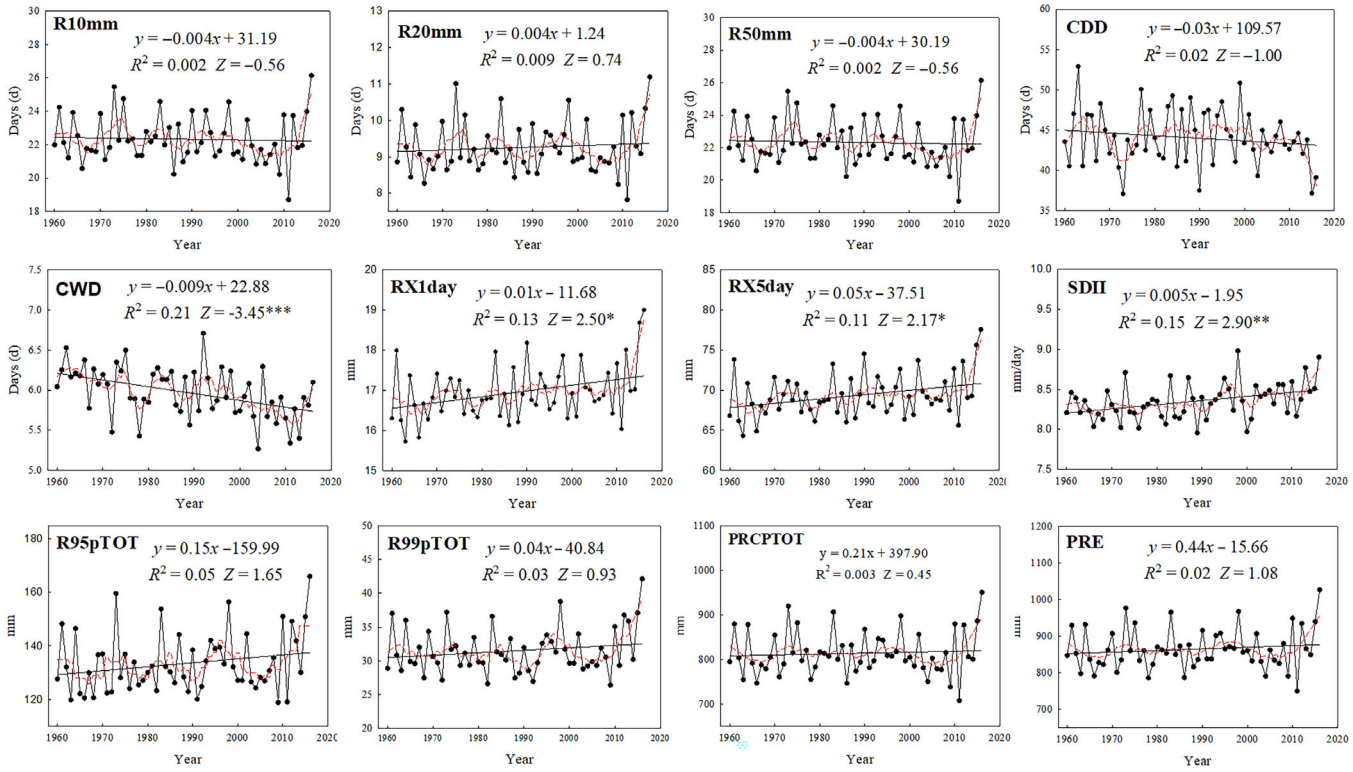

FIGURE 6 Regionally averaged series for the indices of extreme precipitation events in China from 1960 to 2016. The indices are defined in Table S1. Straight lines represent linear regressions; the dashed red line is the smoothed 5-year running average. Significance: ***$p < .001$; **$p < .01$; *$p < .05$; ns, not significant

In contrast, the number of consecutive wet days (CWD) decreased significantly, at a rate of 0.09 days per decade ($p < .001$). Moreover, the monthly maximum 1-day precipitation (RX1day) and maximum consecutive 5-day precipitation (RX5day) increased by 0.1 and 0.5 mm per decade, respectively ($p < .01$).

3.4.2 | Spatial trends in extreme precipitation events

Figure 7 shows that the extreme precipitation indices in most regions of China showed nonsignificant changes from 1960 to 2016. Total annual precipitation (PRCPTOT, the total for daily precipitation >1 mm), heavy precipitation (R10mm), very heavy precipitation (R20mm), monthly maximum 1-day precipitation (RX1day), and maximum consecutive 5-day precipitation (RX5day) showed similar distributions for their trends, with a significant increase in Northwest China and significant decreases in the South Central region. In contrast, the number of consecutive wet days (CWD) increased significantly in the Southern Central region, and decreased in a large area of the Northwest region. The annual precipitation on very wet days (R95pTOT) increased significantly in parts of Northwest region, but decreased slightly in Northeast region and South Central region and showed a nonsignificant increase in the East region. Overall, the precipitation on extremely wet days (R99pTOT) increased more obviously in the eastern half of China than in the west.

3.4.3 | Correlation coefficients for the precipitation indices

We found strong positive correlations between the annual precipitation (Pre, including all rainfall) and the extreme precipitation indices, excluding the consecutive dry days (CDD; Figure 8, $r = -.45$). The correlation coefficients were greater than .85 between the annual precipitation and the extreme precipitation indices heavy precipitation (R10mm), very heavy precipitation (R20mm), rainstorm (R50mm), monthly maximum 1-day precipitation (RX1day), maximum consecutive 5-day precipitation (RX5day), annual precipitation on very wet days (R95pTOT) and annual total wet day precipitation (PRCPTOT, for daily precipitation >1 mm). There were positive correlations among the extreme precipitation indices, but negative correlations between consecutive dry days (CDD) and the precipitation indices.

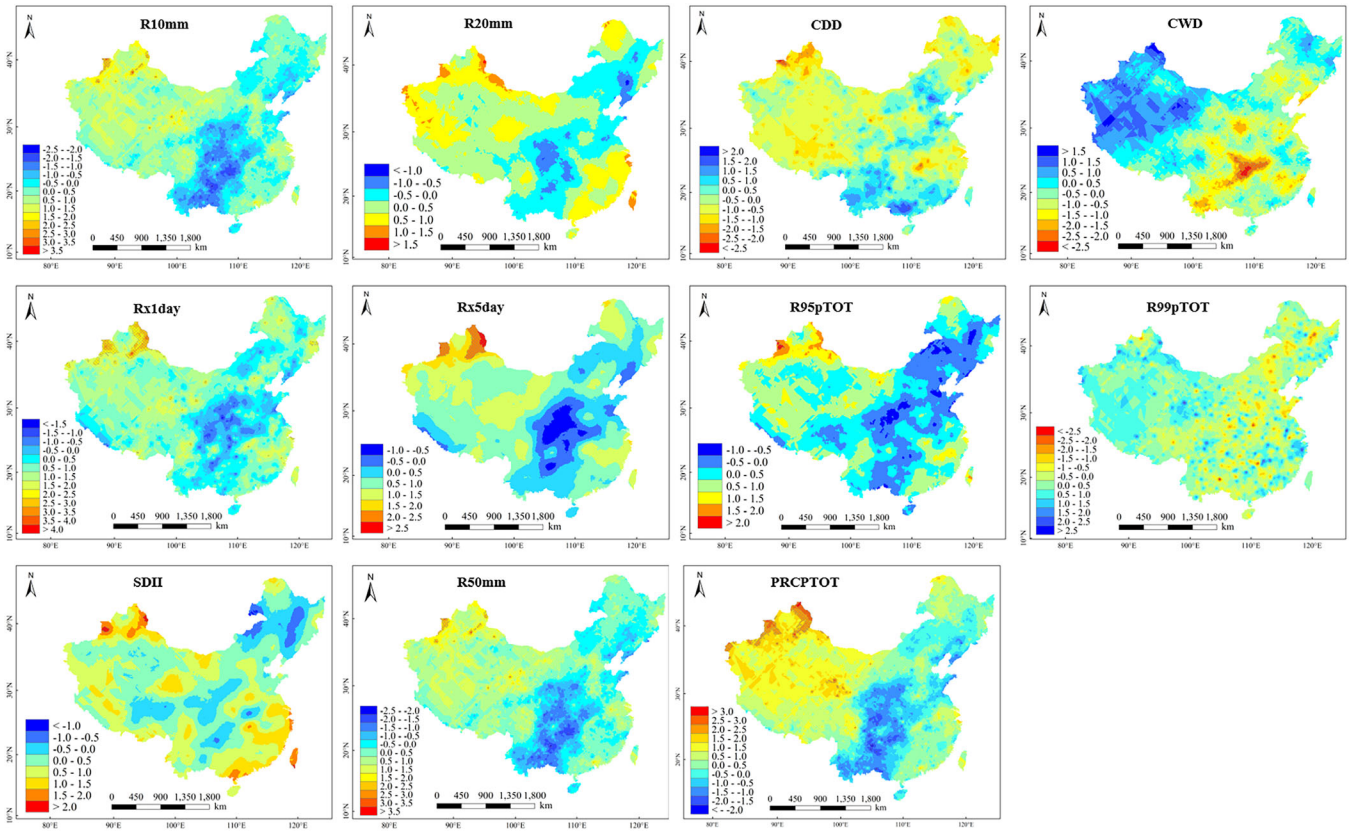

FIGURE 7 Spatial pattern of the Mann–Kendall Z values for precipitation indices from 794 meteorological stations in China from 1960 to 2016. The descriptions of these indices are shown in Table S1. $Z < 0$ represents a decreasing trend, $Z > 0$ represents an increasing trend, and $|Z| > 1.96$ indicates that the trend was statistically significant ($p < .05$). Hatching shows areas where the change trends are significant

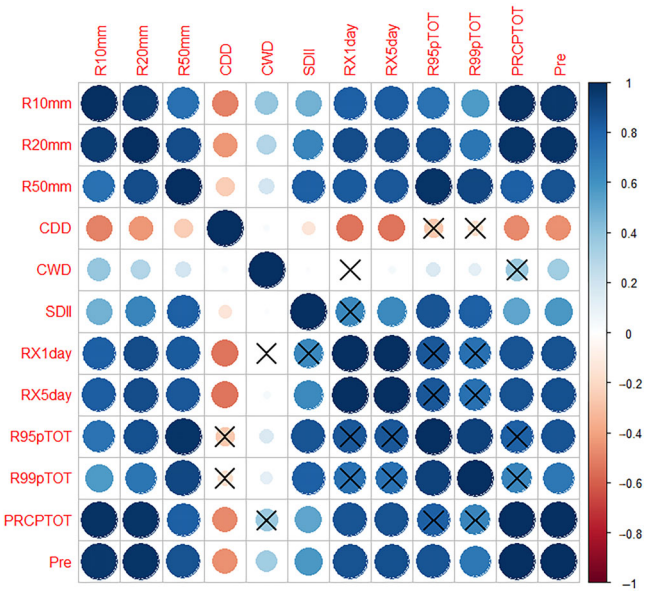

FIGURE 8 Correlations (Pearson's r) among annual precipitation (pre, all rainfall events) and the extreme precipitation indices from 1960 to 2016. The circle size is proportional to the r value, and the X symbol in a cell means a nonsignificant correlation

4 | DISCUSSION

4.1 | Change trends in the extreme temperature and precipitation indices

The occurrences of cold days and cold nights have decreased and the occurrence of warm days and warm nights have increased due to global warming (IPCC, 2007). In the present study, the cool temperature indices generally exhibited significant decreasing trends from 1960 to 2016 in mainland China (that is, there were fewer extreme cold days), whereas the warm temperature indices showed significant increasing trends. This is consistent with similar studies in other regions. For example, at a global scale, 70% of locations showed increases and decreases in the numbers of warm nights and cold nights, respectively (Alexander *et al.*, 2006). Similar research has been implemented in Europe (Klein Tank and Können, 2003), Central and South America (Aguilar *et al.*, 2005), and Africa (New *et al.*, 2006; Gbode *et al.*, 2019), and the extreme temperature indices in these regions showed similar trends. In addition, the strengths

of the trends for the night temperature indices (TN10p and TN90p), were greater than those for the daytime indices (TX10p and TX90p), indicating that nocturnal warming contributed more than daytime warming to the overall warming process. This has been confirmed by other studies (Moberg *et al*., 2006; Revadekar *et al*., 2013; Yan *et al*., 2014). In the present study, the strengths of the trends for the temperature indices were lower than those in the Loess Plateau of northwestern China (Sun *et al*., 2016), the Xinjiang Autonomous Region of northwestern China (Wang *et al*., 2013a), and the Tibetan Plateau of western China (Wang *et al*., 2013b), but greater than those for the Yunnan–Guizhou plateau in southwestern China (Li *et al*., 2012) and the Yangtze River basin in central and southern China (Wang *et al*., 2014). Specifically, the magnitude of the trend for TNn in mainland China was lower than the average value for the Yangtze River Basin (0.42°C·decade^{-1}; Guan *et al*., 2015), the Yellow River Basin (0.45°C·decade^{-1}; Dong *et al*., 2019) and the Yarlung Tsangpo River Basin in China (0.48°C·decade^{-1}; Liu *et al*., 2019). Similarly, the trend for FD (−2.63 days·decade^{-1}) was less than that in the Yellow River Basin (−3.72 days·decade^{-1}; Dong *et al*., 2019), Tibetan Plateau (−5.69 days·decade^{-1}; Sun *et al*., 2016), Loess Plateau (−3.22 days·decade^{-1}; Wang *et al*., 2013b), and Yarlung Tsangpo River Basin (−4.39 days·decade^{-1}; Liu *et al*., 2019), but larger than those in the Wujiang River Basin (−2.19 days·decade^{-1}) and Jialing River Basin (−1.93 days·decade^{-1}) (Wang *et al*., 2014) in China.

Overall, the strengths of the trends for the precipitation indices were lower than those for the temperature indices. The rate of increase of annual total precipitation (PRCPTOT) in this study was higher than those in the Loess Plateau (Sun *et al*., 2016), the Tibetan Plateau (Wang *et al*., 2013b), the Songhua River basin in northeastern China (Song *et al*., 2015), and the Yangtze River basin (Wang *et al*., 2014). In addition, we observed an increasing frequency and intensity of extreme precipitation events, which was consistent with previous work in China (Wang *et al*., 2013b, 2014, 2018; Song *et al*., 2015), excluding the Loess Plateau (Sun *et al*., 2016). The decreasing trend for CWD in the present study was consistent with the results for Xinjiang (Wang *et al*., 2013a) and the Yunnan–Guizhou plateau (Li *et al*., 2012), which are in Northwest and Southwest China, respectively, but contrary to the results in the Loess Plateau (Sun *et al*., 2016), Tibetan Plateau (Wang *et al*., 2013b), and Songhua River (Song *et al*., 2015) in China. In addition, the regionally averaged SDII (0.05 mm·day^{-1}·decade^{-1}) in the present study was larger than the average value for the Xinjiang region (0.04 mm·day^{-1}·decade^{-1}; Wang *et al*., 2013a), the Tibetan Plateau (0.01 mm·day^{-1}·decade^{-1}; Wang *et al*., 2013b), and the Yunnan–Guizhou plateau (0.03 mm·day^{-1}·decade^{-1}; Li *et al*., 2012), but lower than that in the Yellow River Basin (0.06 mm·day^{-1}·decade^{-1}; Dong *et al*., 2019), and Yarlung Tsangpo River Basin (0.10 mm·day^{-1}·decade^{-1}; Liu *et al*., 2019).

Previous researchers generally considered natural climatic variability and anthropogenic forcing to be the main factors influencing extreme temperatures and precipitation (Hegerl *et al*., 2004). Kiktev *et al*. (2003) found that the simulation of temperature extremes could be significantly improved by integrating anthropogenic effects in their model, particularly for greenhouse gases. Christidis *et al*. (2011) separated the anthropogenic and natural factors that influence warm daytime extremes by means of an optimal fingerprinting analysis, and found that anthropogenic global warming caused decreasing severity of cold days and nights, and increasing severity of warm nights. Zhou and Ren (2011) found that urbanization significantly affected the trends of extreme temperature indices in northern China from 1961 to 2008; for instance, urbanization exacerbated the increases for the numbers of summer days, tropical nights, and warm nights, and the decreases for the numbers of cool nights, cool days, and frost days and in the diurnal temperature range. Despite these findings, the reasons for the changes in extreme temperature and precipitation in mainland China should be further addressed. This is particularly true for the parts of western and northwestern China where the density of meteorological stations is low.

4.2 | Relationships between extreme temperature events and geographic factors

We observed large spatial variation in temperature extremes. To clarify the reasons for the different trends in different regions, we analysed the correlations between extreme temperature events and latitude, longitude, and elevation (Table 2).

Latitude affects the solar incidence angle, and thereby influences the distribution of energy over the Earth's surface. In general, higher latitude areas have a lower solar incidence angle, so they receive less heat, leading to colder temperatures. In contrast, the temperatures are higher at lower latitudes because more solar radiation is intercepted. Warming trends tend to be more evident at high latitudes in the Northern Hemisphere (Serreze *et al*., 2000). In the present study, all the temperature indices were significantly correlated with latitude; the cold indices (FD, ID, TN10p, CSDI) and diurnal temperature range (DTR) showed significant positive correlations ($p < .01$), whereas the warm indices (SU, TR, WSDI, TX90p, and TN90p) showed significant negative

TABLE 2 Correlations (Pearson's *r*) between the temperature extremes from 1960 to 2016 and the latitude, longitude, and elevation of the measurement sites in mainland China

Indices	Latitude	Longitude	Elevation
FD	0.80**	−0.18**	0.43**
SU	−0.57**	0.15**	−0.51**
ID	0.84**	0.05 ns	0.12**
TR	−0.71**	0.25**	−0.38**
TX10p	−0.15**	0.19**	0.00 ns
TX90p	−0.34**	0.01 ns	−0.04 ns
TN10p	0.17**	0.19**	0.06 ns
TN90p	−0.26**	−0.20**	0.10**
WSDI	−0.34**	0.19**	−0.21**
CSDI	0.26**	−0.21**	−0.26**
TXx	−0.72**	0.15**	−0.48**
TXn	−0.84**	0.02 ns	−0.31**
TNx	−0.74**	0.25**	−0.51**
TNn	−0.84**	0.13**	−0.38**
DTR	0.60**	−0.38**	0.42**

Note: Significance (two-tailed): **$p < .01$; ns, not significant.

TABLE 3 Correlations (Pearson's *r*) between precipitation extremes from 1960 to 2016 and the latitude, longitude, and elevation of the measurement sites in mainland China

Indices	Latitude	Longitude	Elevation
R10mm	−0.78**	0.37**	−0.27**
R20mm	−0.77**	0.38**	−0.34**
R50mm	−0.72**	0.34**	−0.36**
CDD	0.55**	−0.42**	0.26**
CWD	−0.76**	0.11**	0.11**
SDII	−0.64**	0.58**	−0.43**
RX1day	−0.75**	0.46**	−0.38**
RX5day	−0.76**	0.45**	−0.38**
R95pTOT	−0.78**	0.38**	−0.31**
R99pTOT	−0.74**	0.39**	−0.30**
PRCPTOT	−0.79**	0.36**	−0.27**

Note: Significance (two-tailed): **$p < .01$.

correlations ($p < .01$). This indicates that the warming trend became more significant with decreasing latitude, which was inconsistent with previous research in the Yangtze River Basin (Guan *et al*., 2015) and the Hengduan Mountains of China (Li *et al*., 2012). This difference is likely to have been caused by the different latitude ranges; in the previous research, the study area covered a relatively small range of latitudes, versus all of China in the present study. Furthermore, the extremal indices for the warmest day (TXx), warmest night (TNx), coldest day (TXn), and coldest night (TNn) all showed strong and significant negative correlations with latitude ($p < .01$), indicating that the occurrences of daily extreme temperature events would decrease with increasing latitude.

Longitude affects regional climate change by influencing the transport of water and energy between the coast and China's inland areas (Zhong *et al*., 2017). Brown *et al*. (2010) found that climate change became more significant in coastal areas than inland areas in the northeastern United States. Guan *et al*. (2015) found that cold indices in the Yangtze River basin increased with increasing longitude when the longitude was <112°E, whereas the cold indices decreased with increasing longitude when the longitude was <112°. In the present study, the temperature extremes generally had weaker correlations with longitude than with latitude (Table 2), and there were more nonsignificant correlations. Three warm indices (SU, TR, and WSDI) showed significant positive correlations with longitude ($p < .01$), whereas two cold indices (FD and CSDI) showed significant negative correlations with longitude. This indicated that transport of water and energy between longitudes appears to have relatively little correlation with changes in temperature extremes in mainland China. This might due to the geographical location (e.g., proximity to the Himalayas or to large desert areas) or human activity, but the physical mechanisms responsible for the correlations between longitude and temperature extremes should be further investigated.

Elevation determines the vertical distribution of energy and water, and thereby influences regional climate change. Giorgi *et al*. (1997) found that the warming trend became more significant at high elevations than low elevations in the Austrian Alps. Similar conclusions were obtained in the Rocky Mountains of North America (Fyfe and Flato, 1999), on the Tibetan Plateau (Liu *et al*., 2009), and in southwestern China (Li *et al*., 2012). In the present study, two cold indices (FD and ID) showed significant positive correlations with elevation ($p < .01$), whereas three warm indices (SU, TR, and WSDI) showed significant negative correlations (Table 2). This indicated that the frequency and intensity of cold temperature events increased at high elevations, whereas warm temperature events showed the opposite trend. In addition, the extremal indices for the warmest day (TXx), warmest night (TNx), coldest day (TXn), and coldest night (TNn) all showed significant negative correlations with elevation ($p < .01$), indicating that the occurrences of daily extreme temperature events would decrease with increasing elevation.

TABLE 4 Correlations (Pearson's *r*) between temperature extremes from 1960 to 2016 in mainland China and the atmospheric circulation patterns

Indices	SHA	SHI	SHR	SHW	AO	NAO	PDO	SOI
SU	0.500**	0.479**	−0.059 ns	−0.506**	−0.013 ns	−0.164 ns	−0.063 ns	−0.114 ns
TR	0.604**	0.600**	0.047 ns	−0.575**	0.115 ns	−0.174 ns	−0.067 ns	0.127 ns
FD	−0.655**	−0.630**	0.056 ns	0.683**	−0.296*	−0.056 ns	−0.119 ns	0.117 ns
ID	−0.515**	−0.477**	0.185 ns	0.530**	−0.305*	−0.157 ns	−0.24 ns	0.212 ns
TX10p	−0.474**	−0.444**	0.132 ns	0.473**	−0.128 ns	−0.072 ns	−0.235 ns	0.200 ns
TX90p	0.423**	0.418**	0.073 ns	−0.416**	0.091 ns	−0.123 ns	−0.209 ns	0.100 ns
TN90p	0.481**	0.449**	0.079 ns	−0.479**	0.170 ns	−0.087 ns	−0.085 ns	0.166 ns
TN10p	−0.609**	−0.571**	0.042 ns	0.648**	−0.320*	−0.169 ns	−0.247 ns	0.217 ns
DTR	−0.480**	−0.466**	−0.063 ns	0.503**	−0.355**	−0.152 ns	−0.246 ns	−0.035 ns
CSDI	−0.435**	−0.387**	0.032 ns	0.506**	−0.173 ns	−0.223 ns	−0.294*	0.307*
WSDI	0.339**	0.356**	0.134 ns	−0.308*	0.119 ns	0.001 ns	−0.169 ns	0.042 ns
TXx	0.594**	0.576**	−0.217 ns	−0.582**	−0.057 ns	−0.130 ns	0.098 ns	−0.128 ns
TXn	0.362**	0.336*	0.037 ns	−0.374**	0.369**	0.085 ns	−0.133 ns	0.038 ns
TNx	0.744**	0.722**	−0.163 ns	−0.740**	0.175 ns	−0.029 ns	0.139 ns	−0.078 ns
TNn	0.609**	0.576**	−0.041 ns	−0.630**	0.368**	0.065 ns	0.111 ns	0.013 ns
Tem	0.687**	0.658**	−0.047 ns	−0.702**	0.272*	0.042 ns	0.116 ns	−0.108 ns

Note: Significance (two-tailed): $^{**}p < .01$; $^{*}p < .05$; ns, not significant.

Abbreviations: AO, Arctic Oscillation; NAO, North Atlantic Oscillation; PDO, Pacific Decadal Oscillation; SHA, Subtropical High Area; SHI, Subtropical High Intensity; SHR, Subtropical High Ridge Index; SHW, Subtropical High Western Ridge Point; SOI, Southern Oscillation Index.

4.3 | Relationships between extreme precipitation events and geographic factors

Similarly, we analysed the correlations between extreme precipitation events and latitude, longitude, and elevation (Table 3). All of the precipitation indices showed significant negative correlations with latitude, except for the number of consecutive dry days (CDD). This indicates that the extreme precipitation events were more frequent at low latitudes, probably due mainly to the greater precipitation in low-latitude coastal areas and the low precipitation in high-latitude inland areas, which have large areas of desert. Longitude had the opposite effect on extreme precipitation events, with all of the precipitation indices except CDD showing significant positive correlations with longitude, and CDD showing a negative correlation (Table 3). This may be because the areas with a higher longitude are closer to the coast, where the frequency and intensity of precipitation are higher, whereas areas with a lower longitude are dominated by deserts in northern China. The precipitation indices showed significant negative correlations with elevation (Table 3), except for the two consecutive indices for dry and wet days (CDD and CWD), which showed significant positive correlations. This indicates that the occurrence of extreme precipitation events decreases with increasing elevation.

4.4 | Correlations between temperature extremes and atmospheric circulation patterns

The Subtropical High is an important atmospheric circulation system that links extratropical and tropical circulation (Zhao and Gong, 2002). As one of the most important components of the East Asian monsoon, the West Pacific Subtropical High (WPSH) plays a prominent role in influencing temperature and precipitation conditions in China (Zhao and Wang, 2017). Sun *et al.* (2016) found that the WPSH was positively correlated with warm extremes (SU and TX90p), and negatively correlated with cold extremes (TX10p, TN10p, and FD) on the Loess Plateau (Sun *et al.*, 2016). Zhong *et al.* (2017) also found that the area and intensity of the WPSH showed positive correlations with extremal temperature indices in the Songhua River Basin.

Table 4 shows the correlations between these circulation patterns and the mean annual temperature (Tem) and the other temperature extremal indices. Several warm indices (SU, TR, WSDI, TX90p, and TN90p) showed significant positive correlations with the Subtropical High Intensity (SHI) and Subtropical High Area (SHA), whereas several cold indices (FD, ID, CSDI, TX10p, and TN10p) showed significant negative

correlations. The extremal indices for the warmest day (TXx), warmest night (TNx), coldest day (TXn), and coldest night (TNn) all showed significant positive correlations with SHA and SHI. The correlations between these temperature extremes and the Subtropical High Western Ridge Point (SHW) showed the opposite responses. Therefore, an increase in the area and intensity of the Western Pacific Subtropical High (WPSH) will lead to a significant increase in extreme warm events and a significant decrease in extreme cold events in mainland China. When the SHW moves eastward, the mean temperature and extreme warming indices are likely to decrease significantly, whereas the extreme cold indices are likely to increase significantly. In contrast, the Subtropical High Ridge Index (SHR) had no statistically significant effect on the temperature indices.

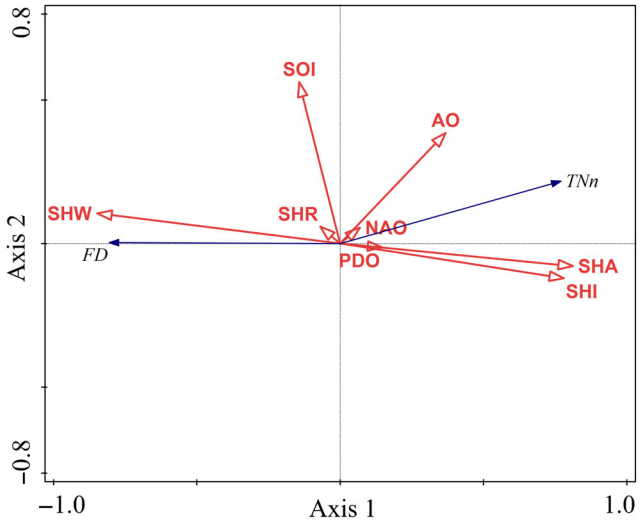

FIGURE 9 Ordination diagram from the redundancy analysis for the relationships between temperature extremes (FD, the number of frost days; TNn, the minimum daily minimum temperature) and the atmospheric circulation patterns. AO, Arctic Oscillation; NAO, North Atlantic Oscillation; PDO, Pacific Decadal Oscillation; SHA, Subtropical High Area; SHI, Subtropical High Intensity; SHR, Subtropical High Ridge Index; SHW, Subtropical High Western Ridge Point; SOI, Southern Oscillation Index

The Arctic Oscillation (AO) is a dominant control of climate over the extratropical regions of the Northern Hemisphere (Thompson and Wallace, 1998), and the AO is closely related to the Siberian high pressure system and the East Asian winter monsoon, both of which strongly affect China's climate (You *et al.*, 2013). Many researchers have studied the correlations between the AO and temperature extremes around the world (Thompson and Wallace, 2001; Jeong and Ho, 2005; Park *et al.*, 2010). He and Wang (2016) found that the AO index was significantly negatively correlated with the numbers of cold days and cold nights, and Sun *et al.* (2016) reached similar conclusions for the Loess Plateau. In the present study, the AO index showed significant negative correlations with the numbers of frost days (FD), ice days (ID), and cool nights (TN10p) and with the diurnal temperature range (DTR). There were also significant positive correlations between the AO index and the mean annual temperature (Tem) and two daily extremal cold indices

TABLE 5 Correlations (Pearson's *r*) between precipitation extremes from 1960 to 2016 in mainland China and the atmospheric circulation patterns

Indices	SHA	SHI	SHR	SHW	AO	NAO	PDO	SOI
RX1day	0.529**	0.556**	−0.06 ns	−0.494**	0.245	0.035 ns	0.277*	−0.25 ns
RX5day	0.490**	0.520**	−0.037 ns	−0.459**	0.240 ns	0.016 ns	0.252 ns	−0.233 ns
R20mm	0.421**	0.455**	−0.055 ns	−0.343**	0.066 ns	−0.157 ns	0.208 ns	−0.147 ns
R50mm	0.291*	0.338*	−0.003 ns	−0.207 ns	0.07 ns	−0.123 ns	0.200 ns	−0.172 ns
CDD	−0.265*	−0.289*	−0.156 ns	0.251 ns	−0.254 ns	−0.114 ns	−0.092 ns	0.003 ns
CWD	−0.22 ns	−0.183 ns	−0.121 ns	0.263*	−0.144 ns	−0.213 ns	0.054 ns	−0.037 ns
R95pTOT	0.516**	0.544**	−0.004 ns	−0.441**	0.022 ns	−0.150 ns	0.224 ns	−0.073 ns
R99pTOT	0.463**	0.506**	0.082 ns	−0.351**	−0.02 ns	−0.117 ns	0.134 ns	−0.012 ns
PRCPTOT	0.244 ns	0.293*	0.044 ns	−0.164 ns	0.085 ns	−0.119 ns	0.167 ns	−0.130 ns
R10mm	0.291*	0.338*	−0.003 ns	−0.207 ns	0.070 ns	−0.123 ns	0.200 ns	−0.172 ns
SDII	0.700**	0.685**	−0.219 ns	−0.661**	−0.066 ns	−0.176 ns	0.287*	−0.125 ns
Pre	0.416**	0.461**	−0.005 ns	−0.326*	0.061 ns	−0.160 ns	0.170 ns	−0.092 ns

Note: Significance (two-tailed): $^{**}p < .01$; $^{*}p < .05$; ns, not significant.

Abbreviations: AO, Arctic Oscillation; NAO, North Atlantic Oscillation; PDO, Pacific Decadal Oscillation; SHA, Subtropical High Area; SHI, Subtropical High Intensity; SHR, Subtropical High Ridge Index; SHW, Subtropical High Western Ridge Point; SOI, Southern Oscillation Index.

(TXn and TNn). The AO was not significantly related to the other indices.

Moreover, the North Atlantic Oscillation (NAO), Southern Oscillation Index (SOI), and Pacific Decadal Oscillation (PDO) showed few significant correlations with the extreme temperature indices. The PDO index was significantly negatively correlated with CSDI, whereas SOI was significantly positively correlated with CSDI.

4.5 | Summary of the atmospheric circulation patterns that influence the temperature extremes

We selected the indices with the strongest increasing and decreasing trends from the temperature extremes, and then used the ordination diagram produced by RDA to summarize the factors that influence the variation in temperature extremes (Figure 9). The eigenvalues of axis 1 and axis 2 were 0.6487 and 0.0008, respectively, and the cumulative proportion of the variation explained by the eight circulation patterns was 65.0%. FD was positively associated with SHW, SHR, and SOI, but negatively associated with SHA, SHI, AO, PDO, and NAO; TNn showed the opposite relationships. We used a partial Monte Carlo permutation test to evaluate the contributions of each circulation pattern to the variation of FD and TNn (Table S3). The SHW explained the largest proportion of the variation (46.5%), and also had the highest contribution rate (71.6%). The influences of AO and PDO were statistically significant, but much smaller. The effects of SHR, NAO, SOI, SHA, and SHI were small and not statistically significant. This showed that SHW was the dominant driver for the variation of extreme temperature events in mainland China.

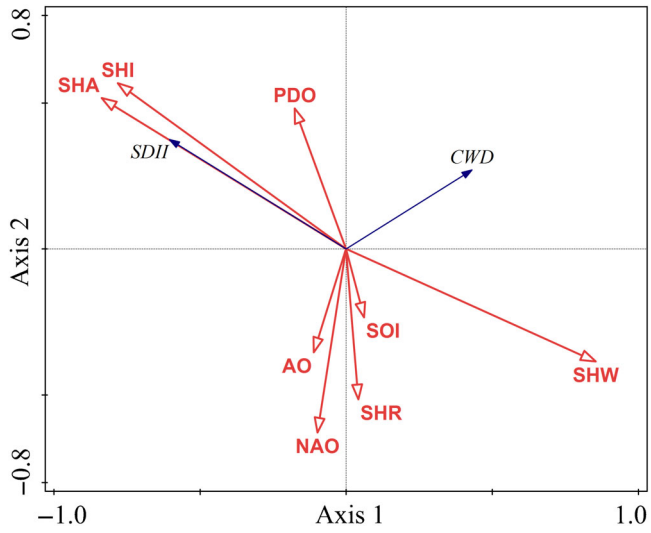

FIGURE 10 Ordination diagram of the redundancy analysis for precipitation extremes (SDII and CWD) with atmospheric circulation patterns. AO, Arctic Oscillation; NAO, North Atlantic Oscillation; PDO, Pacific Decadal Oscillation; SHA, Subtropical High Area; SHI, Subtropical High Intensity; SHR, Subtropical High Ridge Index; SHW, Subtropical High Western Ridge Point; SOI, Southern Oscillation Index

4.6 | Correlations between the precipitation extremes and the atmospheric circulation patterns

Table 5 shows fewer significant correlations between the precipitation parameters and the circulation patterns than was the case for the temperature parameters. The Subtropical High Intensity (SHI) and Subtropical High Area (SHA) showed significant positive correlations with all the precipitation extremes, except for negative correlations with the two consecutive indices (CWD and CDD). This indicates that the number and intensity of extreme precipitation events increased with increasing intensity and area of the West Pacific Subtropical High. The Western Ridge Point (SHW) was significantly negatively correlated with precipitation extremes, excluding CDD and CWD, which indicates that when the SHW moves eastward, extreme precipitation events are likely to decrease significantly, whereas the extreme precipitation events would increase if SHW moves westward. The other circulation indices showed no significant correlations with the extreme precipitation indices, except for positive correlations between the PDO index and both RX1day and SDII.

4.7 | Summary of the atmospheric circulation patterns that influence the precipitation extremes

Similarly, we summarized the factors that influence the variation in temperature extremes with the most obvious change trends using redundancy analysis (Figure 10). The eigenvalues of axis 1 and axis 2 were 0.2466 and 0.0962, respectively, and the cumulative proportion of the variation explained by the eight circulation patterns was 34.3% (Table S4). SDII was positively associated with SHA, SHI, and PDO, but negatively associated with SHW, SHR, AO, NAO, and SOI; CWD showed the opposite relationships with SHW, SHA, and SHI. The SHA explained the largest proportion of the variation (19.8%), and also had the highest contribution rate (57.8%). The effects of the remaining atmospheric circulation patterns were small and not statistically significant, indicating

that SHA played a prominent role in extreme precipitation events in mainland China.

5 | CONCLUSIONS

In this study, we used 15 extreme temperature indices and 11 extreme precipitation indices to quantify the changes in climate extremes in mainland China from 1960 to 2016. The regionally averaged trends for the temperature indices were consistent with global warming. The warmth indices, including the numbers of warm days, warm nights, summer days, and tropical nights, showed significantly increasing trends during the study period. In contrast, the cold indices, including the numbers of cool days, cool nights, ice days, and frost days decreased significantly. Furthermore, the extremal daily indices, including the warmest day, warmest night, coldest day, and coldest night, showed significant increasing trends during the same period. The warmth indices and extreme daily indices showed significant negative correlations with latitude, indicating that the warming trend became more significant at lower latitudes, whereas the warming trend became more significant with increasing longitude, largely due to proximity to the eastern coast of China. In addition, the magnitudes of the warmth indices and extreme daily indices decreased with increasing elevation, whereas the frequency and intensity of extreme cold events increased at high elevations.

The daily rainfall intensity increased significantly from 1960 to 2016, whereas the number of consecutive wet days decreased significantly. Furthermore, the maximum 1-day precipitation, maximum consecutive 5-day precipitation, and the precipitation on extremely wet days also increased significantly. The number and intensity of extreme precipitation events decreased significantly with increasing latitude, but increased significantly with increasing longitude. Furthermore, the number and intensity of extreme precipitation events decreased with increasing elevation.

Large-scale atmospheric circulation patterns, represented by indices for each circulation pattern, sometimes strongly affected the climate extremes. The Arctic Oscillation, the Western Pacific Subtropical High Intensity and Area indices, and the Western Ridge Point index strongly influenced the extremes and contributed significantly to the climate in mainland China. Specifically, the increasing area and intensity of the Western Pacific Subtropical High led to significant increases in temperature and extreme warm events, and significant decreases in extreme cold events in mainland China. When the Western Ridge Point moves eastward, the extreme warming indices are likely to decrease significantly, whereas the extreme cold indices are likely to increase significantly. In addition, extreme precipitation events increased with increasing intensity and area of the Western Pacific Subtropical High. The extreme precipitation events are likely to decrease when the Subtropical High Western Ridge Point moves eastward, whereas the extreme precipitation events would increase if this point moves westward.

ACKNOWLEDGEMENTS

This research was supported by the National Key R and D Program of China (2017YFA0604803 and 2016YFC0500901), the National Natural Science Foundation of China (grants 31971466 and 41807525), and the Strategic Priority Research Program of the Chinese Academy of Sciences (XDA23060404).

CONFLICT OF INTEREST

The authors declare that they have no conflict of interest.

ORCID

Yuqiang Li https://orcid.org/0000-0001-5264-8122

REFERENCES

Aguilar, E., Peterson, T.C., Obando, P.R., Frutos, R., Retana, J.A., Solera, M., Soley, J., García, I.G., Araujo, R.M., Santos, A.R., Valle, V.E., Brunet, M., Aguilar, L., Álvarez, L., Bautista, M., Castañón, C., Herrera, L., Ruano, E., Sinay, J.J., Sánchez, E., Oviedo, G.I.H., Obed, F., Salgado, J.E., Vázquez, J.L., Baca, M., Gutiérrez, M., Centella, C., Espinosa, J., Martínez, D., Olmedo, B., Espinoza, C.E.O., Núñez, R., Haylock, M., Benavides, H. and Mayorga, R. (2005) Changes in precipitation and temperature extremes in Central America and northern South America, 1961–2003. *Journal of Geophysical Research*, 110, D23107.

Alexander, L.V., Zhang, X.B., Peterson, T.C., Caesar, J. and Vazquez-Aguirre, J.L. (2006) Global observed changes in daily climate extremes of temperature and precipitation. *Journal of Geophysical Research: Atmospheres*, 111, 1042–1063.

Barriopedro, D., Fischer, E.M., Luterbacher, J., Trigo, R.M. and Garcia-Herrera, R. (2011) The hot summer of 2010: redrawing the temperature record map of Europe. *Science*, 332(6026), 220–224.

Becker, A. and Grünewald, U. (2003) Disaster management: flood risk in Central Europe. *Science*, 300, 1099.

Brown, P.J., Bradley, R.S. and Keimig, F.T. (2010) Changes in extreme climate indices for the northeastern United States, 1870–2005. *Journal of Climate*, 23, 6555–6572.

Christidis, N., Stott, P.A. and Brown, S.J. (2011) The role of human activity in the recent warming of extremely warm daytime temperatures. *Journal of Climate*, 24(7), 1922–1930.

Coumou, D. and Rahmstorf, S. (2012) A decade of weather extremes. *Nature Climate Change*, 2, 491–496.

Croitoru, A.E., Chiotoroiu, B.C., Ivanova, V. and Torica, V. (2013) Changes in precipitation extremes on the Black Sea Western Coast. *Global and Planetary Change*, 102, 10–19.

Donat, M.G., Alexander, L.V., Yang, H., Durre, I. and Caesar, J. (2013) Global land-based datasets for monitoring climatic

extremes. *Bulletin of the American Meteorological Society*, 94(7), 997–1006.

Dong, X., Zhang, S., Zhou, J., Cao, J. and Liu, Y. (2019) Magnitude and frequency of temperature and precipitation extremes and the associated atmospheric circulation patterns in the Yellow River basin (1960–2017), China. *Water*, 11(11), 2334.

Dos Santos, C.A.C., Neale, C.M.U., Rao, T.V.R. and da Silva, B.B. (2011) Trends in indices for extremes in daily temperature and precipitation over Utah, USA. *International Journal of Climatology*, 31, 1813–1822.

Filahi, S., Tanarhte, M., Mouhir, L., El Morhit, M. and Tramblay, Y. (2016) Trends in indices of daily temperature and precipitations extremes in Morocco. *Theoretical and Applied Climatology*, 124, 959–972.

Founda, D. and Giannakopoulos, C. (2009) The exceptionally hot summer of 2007 in Athens, Greece—a typical summer in the future climate? *Global and Planetary Change*, 67, 227–236.

Frich, P., Alexander, L.V., Della-Marta, P., Gleason, B., Haylock, M., Klein Tank, A.M.G. and Peterson, T. (2002) Observed coherent changes in climatic extremes during the second half of the twentieth century. *Climate Research*, 19(3), 193–212.

Fyfe, J.C. and Flato, G.M. (1999) Enhanced climate change and its detection over the Rocky Mountains. *Journal of Climate*, 12(1), 230–243.

Gbode, I.E., Adeyeri, O.E., Menang, K.P., Intsiful, J.D.K., Ajayi, V. O., Omotosho, J.A. and Akinsanola, A.A. (2019) Observed changes in climate extremes in Nigeria. *Meteorological Applications*, 26(4), 642–654.

Gerken, T., Bromley, G., Ruddell, B., Williams, S. and Stoy, P. (2018) Convective suppression before and during the United States northern great plains flash drought of 2017. *Hydrology and Earth System Sciences*, 22, 4155–4163.

Giorgi, F., Hurrell, J.W., Marinucci, M.R. and Beniston, M. (1997) Elevation dependency of the surface climate change signal: a model study. *Journal of Climate*, 10, 288–296.

Griffiths, G.M., Chambers, L.E., Haylock, M.R., Manton, M.J., Nicholls, N., Baek, H.J., Choi, Y., Della-Marta, P.M., Gosai, A., Iga, N., Lata, R., Laurent, V., Maitrepierre, L., Nakamigawa, H., Ouprasitwong, N., Solofa, D., Tahani, L., Thuy, D.T., Tibig, L., Trewin, B., Vediapan, K. and Zhai, P. (2005) Change in mean temperature as a predictor of extreme temperature change in the Asia-Pacific region. *International Journal of Climatology*, 25, 1301–1330.

Groisman, P.Y., Karl, T.R., Easterling, D.R., Knight, R.W., Jamason, P.F., Hennessy, K.J., Suppiah, R., Page, C.M., Wibig, J., Fortuniak, K., Razuvaev, V.N., Douglas, A., Førland, E. and Zhai, P.M. (1999) Changes in the probability of heavy precipitation: important indicators of climatic change. *Climatic Change*, 42, 243–283.

Guan, Y., Zhang, X., Zheng, F. and Wang, B. (2015) Trends and variability of daily temperature extremes during 1960-2012 in the Yangtze River basin, China. *Global and Planetary Change*, 124, 79–94.

Hamed, K.H. and Rao, A.R. (1998) A modified Mann–Kendall trend test for autocorrelated data. *Journal of Hydrology*, 204, 182–196.

Haylock, M.R., Peterson, T.C., Alves, L.M., Ambrizzi, T., Anunciação, Y.M.T., Baez, J., Barros, V.R., Berlato, M.A., Bidegain, M., Coronel, G., Corradi, V., Garcia, V.J., Grimm, A. M., Karoly, D., Marengo, J.A., Marino, M.B., Moncunill, D.F., Nechet, D., Quintana, J., Rebello, E., Rusticucci, M., Santos, J. L., Trebejo, I. and Vincent, L.A. (2006) Trends in total and extreme South American rainfall in 1960–2000 and links with sea surface temperature. *Journal of Climate*, 19(8), 1490–1512.

He, S. and Wang, H. (2016) Linkage between the east Asian January temperature extremes and the preceding Arctic oscillation. *International Journal of Climatology*, 36(2), 1026–1032.

Hegerl, G.C., Zwiers, F.W., Stott, P.A. and Kharin, V.V. (2004) Detectability of anthropogenic changes in annual temperature and precipitation extremes. *Journal of Climate*, 17, 3683–3700.

Hoerling, M., Eischeid, J., Kumar, A., Leung, R., Mariotti, A., Mo, K., Schubert, S. and Seager, R. (2014) Causes and predictability of the 2012 great plains drought. *Bulletin of the American Meteorological Society*, 95(2), 269–282.

Houghton, J.T., Ding, Y., Griggs, D.J., Noguer, M., Linden, P.J., Dai, X., Maskell, K. and Johnson, C.A. (2001) Observed climate variability and change. In: *Climate Change 2001: The Science of Climate Change*. Cambridge, UK: Cambridge University Press, pp. 156–159.

Insaf, T.Z., Lin, S. and Sheridan, S.C. (2013) Climate trends in indices for temperature and precipitation across New York state, 1948–2008. *Air Quality, Atmosphere & Health*, 6, 247–257.

IPCC. (2007) *Climate Change 2007: The Physical Science Basis*. Cambridge: Cambridge University Press.

IPCC. (2013) *Climate Change 2013: The Physical Science Basis*. Cambridge: Cambridge University Press.

IPCC. (2014) Climate change 2014: synthesis report. In: Pachauri, R.K. and Meyer, L.A. (Eds.) *Contribution of Working Groups I, II and III to the Fifth Assessment Report of the Intergovernmental Panel on Climate Change*. Geneva: IPCC, p. 151.

Jeong, J. and Ho, C. (2005) Changes in occurrence of cold surges over East Asia in association with Arctic oscillation. *Geophysical Research Letters*, 32, L14704.

Karoly, D. (2009) The recent bushfires and extreme heat wave in Southeast Australia. *Bulletin of the American Meteorological Society*, 22, 10–13.

Kendall, M.G. (1990) Rank correlation methods. *British Journal of Psychology*, 25, 86–91.

Kiktev, D., Sexton, D.M.H., Alexander, L. and Folland, C.K. (2003) Comparison of modeled and observed trends in indices of daily climate extremes. *Journal of Climate*, 16, 3560–3571.

Klein Tank, A.M.G. and Können, G.P. (2003) Trends in indices of daily temperature and precipitation extremes in Europe, 1946–99. *Journal of Climate*, 16, 3665–3680.

Klein Tank, A., Zwiers, F. and Zhang, X. (2009) Guidelines on analysis of extremes in a changing climate in support of informed decisions for adaptation. *World Meteorological Organization (WCDMP-72, WMO-TD/No.1500)*, 56.

Li, Z., He, Y., Wang, C., Wang, X., Xin, H., Zhang, W. and Cao, W. (2011) Spatial and temporal trends of temperature and precipitation during 1960–2008 at the Hengduan Mountains, China. *Quaternary International*, 236, 127–142.

Li, Z., He, Y., Wang, P., Theakstone, W.H., An, W., Wang, X., Lu, A., Zhang, W. and Cao, W. (2012) Changes of daily climate extremes in southwestern China during 1961–2008. *Global and Planetary Change*, 80–81, 255–272.

Li, Y., He, D., Hu, J. and Cao, J. (2015) Variability of extreme precipitation over Yunnan Province, China 1960–2012. *International Journal of Climatology*, 35, 245–258.

Liu, X., Cheng, Z., Yan, L. and Yin, Z. (2009) Elevation dependency of recent and future minimum surface air temperature trends in the Tibetan plateau and its surroundings. *Global and Planetary Change*, 68, 164–174.

Liu, C., Li, Y., Ji, X., Luo, X. and Zhu, M. (2019) Observed changes in temperature and precipitation extremes over the Yarlung Tsangpo River basin during 1970–2017. *Atmosphere*, 10, 815.

Lu, H., Chen, S., Guo, Y., He, H. and Xu, S. (2014) Spatio-temporal variation characteristics of extremely heavy precipitation frequency over South China in the last 50years. *Journal of Tropical Meteorology*, 20, 279–288.

Luterbacher, J. (2004) European seasonal and annual temperature variability, trends, and extremes since 1500. *Science*, 303, 1499–1503.

Mazdiyasni, O. and AghaKouchak, A. (2015) Substantial increase in concurrent droughts and heatwaves in the United States. *Proceedings of the National Academy of Sciences of the United States of America*, 112, 11484–11489.

Meehl, G.A., Karl, T., Easterling, D.R., Changnon, S., Pielke, R., Changnon, D., Evans, J., Groisman, P.Ya., Knutson, T.R., Kunkel, K.E., Mearns, L.O., Parmesan, C., Pulwarty, R., Root, T., Sylves, R.T., Whetton, P. and Zwiers, F. (2000) An introduction to trends in extreme weather and climate events: observations, socioeconomic impacts, terrestrial ecological impacts, and model projections. *Bulletin of the American Meteorological Society*, 81, 413–416.

Moberg, A., Jones, P.D., Lister, D., Walther, A., Brunet, M., Jacobeit, J., Alexander, L.V., Della-Marta, P.M., Luterbacher, J., Yiou, P., Chen, D., Klein Tank, A.M.G., Saladié, O., Sigró, J., Aguilar, E., Alexandersson, H., Almarza, C., Auer, I., Barriendos, M., Begert, M., Bergström, H., Böhm, R., Butler, C.J., Caesar, J., Drebs, A., Founda, D., Gerstengarbe, F., Micela, G., Maugeri, M., Österle, H., Pandzic, K., Petrakis, M., Srnec, L., Tolasz, R., Tuomenvirta, H., Werner, P.C., Linderholm, H., Philipp, A., Wanner, H. and Xoplaki, E. (2006) Indices for daily temperature and precipitation extremes in Europe analyzed for the period 1901–2000. *Journal of Geophysical Research*, 111 (D22), 106–125.

Mueller, B. and Seneviratne, S.I. (2012) Hot days induced by precipitation deficits at the global scale. *Proceedings of the National Academy of Sciences of the United States of America*, 109, 12398–12403.

New, M., Hewitson, B., Stephenson, D.B., Tsiga, A. and Lajoie, R. (2006) Evidence of trends in daily climate extremes over southern and west Africa. *Journal of Geophysical Research: Atmospheres*, 111, 3007–3021.

Ning, B., Yang, X. and Chang, L. (2012) Changes of temperature and precipitation extremes in Hengduan Mountains, Qinghai-Tibet plateau in 1961–2008. *Chinese Geographical Science*, 22, 422–436.

Park, T., Ho, C., Yang, S. and Jeong, J. (2010) Influences of Arctic oscillation and Madden-Julian oscillation on cold surges and heavy snowfalls over Korea: a case study for the winter of 2009–2010. *Journal of Geophysical Research*, 115, D23122.

Pezza, A.B. and Simmonds, I. (2005) The first South Atlantic hurricane: unprecedented blocking, low shear and climate change. *Geophysical Research Letters*, 32, 1–5.

Powell, E.J. and Keim, B.D. (2015) Trends in daily temperature and precipitation extremes for the southeastern United States: 1948–2012. *Journal of Climate*, 28, 1592–1612.

Revadekar, J.V., Hameed, S., Collins, D., Manton, M., Sheikh, M., Borgaonkar, H.P., Kothawale, D.R., Adnan, M., Ahmed, A.U., Ashraf, J., Baidya, S., Islam, N., Jayasinghearachchi, D., Manzoor, N., Premalal, K.H.M.S. and Shreshta, M.L. (2013) Impact of altitude and latitude on changes in temperature extremes over South Asia during 1971–2000. *International Journal of Climatology*, 33, 199–209.

Serreze, M.C., Walsh, J.E., Chapin III, F.S., Osterkamp, T., Dyurgerov, M., Romanovsky, V., Oechel, W.C., Morison, J., Zhang, T. and Barry, R.G. (2000) Observational evidence of recent change in the northern high-latitude environment. *Climatic Change*, 46, 159–207.

Song, X., Song, S., Sun, W., Mu, X., Wang, S., Li, J. and Li, Y. (2015) Recent changes in extreme precipitation and drought over the Songhua River Basin, China, during 1960–2013. *Atmospheric Research*, 157, 137–152.

Sun, W., Mu, X., Song, X., Wu, D., Cheng, A. and Qiu, B. (2016) Changes in extreme temperature and precipitation events in the Loess plateau (China) during 1960–2013 under global warming. *Atmospheric Research*, 168, 33–48.

Supari, F.T., Liew, J. and Aldrian, E. (2016) Observed changes in extreme temperature and precipitation over Indonesia. *International Journal of Climatology*, 37, 1979–1997.

Tabari, H., Shifteh Somee, B. and Rezaeianzadeh, M. (2011) Testing for long-term trends in climatic variables in Iran. *Atmospheric Research*, 100, 132–140.

Thompson, D.W.J. and Wallace, J.M. (1998) The Arctic oscillation signature in the wintertime geopotential height and temperature fields. *Geophysical Research Letters*, 25, 1297–1300.

Thompson, D.W.J. and Wallace, J.M. (2001) Regional climate impacts of the Northern Hemisphere annular mode. *Science*, 293, 85–89.

Trenberth, K.E. (2011) Changes in precipitation with climate change. *Climate Research*, 47, 123–138.

Viola, F., Liuzzo, L., Noto, L., Conti, F. and la Loggia, G. (2014) Spatial distribution of temperature trends in Sicily. *International Journal of Climatology*, 34, 1–17.

Wang, X.L. (2008a) Accounting for autocorrelation in detecting mean shifts in climate data series using the penalized maximal *t* or *F* test. *Journal of Applied Meteorology and Climatology*, 47, 2423–2444.

Wang, X.L. (2008b) Penalized maximal *F* test for detecting undocumented mean shift without trend change. *Journal of Atmospheric and Oceanic Technology*, 25, 368–384.

Wang, X.L., Wen, Q.H. and Wu, Y. (2007) Penalized maximal *t* test for detecting undocumented mean change in climate data series. *Journal of Applied Meteorology and Climatology*, 46, 916–931.

Wang, B., Zhang, M., Wei, J., Wang, S., Li, S., Ma, Q., Li, X. and Pan, S. (2013a) Changes in extreme events of temperature and precipitation over Xinjiang, Northwest China, during 1960–2009. *Quaternary International*, 298, 141–151.

Wang, S., Zhang, M., Wang, B., Sun, M. and Li, X. (2013b) Recent changes in daily extremes of temperature and precipitation over the western Tibetan plateau, 1973–2011. *Quaternary International*, 313–314, 110–117.

Wang, Q., Zhang, M., Wang, S., Qian, M.A. and Sun, M. (2014) Changes in temperature extremes in the Yangtze River basin, 1962–2011. *Journal of Geographical Sciences*, 24, 59–75.

Wang, X.Y., Li, Y., Chen, Y., Lian, J., Luo, Y., Niu, Y., Gong, X. and Yu, P. (2018) Temporal and spatial variation of extreme temperatures in an agro-pastoral ecotone of northern China from 1960 to 2016. *Scientific Reports*, 8, 8787.

Webster, P.J., Toma, V.E. and Kim, H. (2011) Were the 2010 Pakistan floods predictable? *Geophysical Research Letters*, 38, L04806.

WMO. (2011) World Meteorological Organization provisional statement on the status of the global climate. Available at: http://www.wmo.int/pages/mediacentre/press_releases/gcs_2011_en.html [Accessed February 5, 2020].

WMO. (2016) World Meteorological Organization provisional statement on the status of the global climate. Available at: https://reliefweb.int/report/world/provisional-wmo-statement-status-global-climate-2016 [Accessed February 6, 2020].

Yan, H.M., Chen, W.N., Yang, F.X., Liu, J.Y. and Ji, Y.Z. (2014) The spatial and temporal analysis of extreme climatic events in Inner Mongolia during the past 50 years. *Geographical Research*, 33, 14–22.

You, Q.L., Ren, G., Fraedrich, K., Kang, S., Ren, Y. and Wang, P. (2013) Winter temperature extremes in China and their possible causes. *International Journal of Climatology*, 33, 1444–1455.

Yuan, X., Ma, Z., Pan, M. and Shi, C. (2015) Microwave remote sensing of short-term droughts during crop growing seasons. *Geophysical Research Letters*, 42, 4394–4401.

Yuan, X., Wang, L. and Wood, E.F. (2018) Anthropogenic intensification of southern African flash droughts as exemplified by the 2015/16 season. *Bulletin of the American Meteorological Society*, 99, 86–90.

Zhang, X., Aguilar, E., Sensoy, S., Melkonyan, H., Tagiyeva, U., Ahmed, N., Kutaladze, N., Rahimzadeh, F., Taghipour, A., Hantosh, T.H., Albert, P., Semawi, M., Karam Ali, M., Said Al-Shabibi, M.H., Al-Oulan, Z., Zatari, T., Al Dean Khelet, I., Hamoud, S., Sagir, R., Demircan, M., Eken, M., Adiguzel, M., Alexander, L., Peterson, T.C. and Wallis, T. (2005) Trends in Middle East climate extreme indices from 1950 to 2003. *Journal of Geophysical Research*, 110, 104.

Zhao, X. and Gong, D.Y. (2002) Interdecadal change in Western Pacific subtropical high and climatic effects. *Journal of Geographical Sciences*, 12, 202–209.

Zhao, Z. and Wang, Y. (2017) Influence of the West Pacific subtropical high on surface ozone daily variability in summertime over eastern China. *Atmospheric Environment*, 170, 197–204.

Zhen, Y. and Li, X. (2014) Recent trends in daily temperature extremes over northeastern China (1960–2011). *Quaternary International*, 380–381, 35–48.

Zhong, K., Zheng, F., Wu, H., Qin, C. and Xu, X. (2017) Dynamic changes in temperature extremes and their association with atmospheric circulation patterns in the Songhua River Basin, China. *Atmospheric Research*, 190, 77–88.

Zhou, Y. and Ren, G. (2011) Change in extreme temperature event frequency over mainland China, 1961–2008. *Climate Research*, 50, 125–139.

Zscheischler, J., Westra, S., Van Den Hurk, B.J.J.M., Seneviratne, S.I., Ward, P.J., Pitman, A., AghaKouchak, A., Bresch, D.N., Leonard, M., Wahl, T. and Zhang, X. (2018) Future climate risk from compound events. *Nature Climate Change*, 8, 469–477.

SUPPORTING INFORMATION

Additional supporting information may be found online in the Supporting Information section at the end of this article.

How to cite this article: Wang X, Li Y, Wang M, *et al.* Changes in daily extreme temperature and precipitation events in mainland China from 1960 to 2016 under global warming. *Int J Climatol*. 2020; 1–19. https://doi.org/10.1002/joc.6865